

Article

# Prediction of State-of-Health for Nickel-Metal Hydride Batteries by a Curve Model Based on Charge-Discharge Tests

Huan Yang <sup>1,2</sup>, Yubing Qiu <sup>1,\*</sup> and Xingpeng Guo <sup>1,2</sup>

Received: 24 June 2015 ; Accepted: 27 October 2015 ; Published: 4 November 2015  
Academic Editor: Izumi Taniguchi

<sup>1</sup> School of Chemistry and Chemical Engineering, Huazhong University of Science and Technology, Wuhan 430074, China; lyyanghuan@163.com (H.Y.); guoxp@mail.hust.edu.cn (X.G.)

<sup>2</sup> Key laboratory of Material Chemistry for Energy Conversion and Storage, Huazhong University of Science and Technology, Ministry of Education, Wuhan 430074, China

\* Correspondence: qiuyubin@mail.hust.edu.cn; Tel.: +86-27-8755-9068

**Abstract:** Based on charge-discharge cycle tests for commercial nickel-metal hydride (Ni-MH) batteries, a nonlinear relationship is found between the discharging capacity ( $C_{\text{discharge}}$ , Ah) and the voltage changes in 1 s occurring at the start of the charging process ( $\Delta V_{\text{charge}}$ , mV). This nonlinear relationship between  $C_{\text{discharge}}$  and  $\Delta V_{\text{charge}}$  is described with a curve equation, which can be determined using a nonlinear least-squares method. Based on the curve equation, a curve model for the state-of-health (SOH) prediction is constructed without battery models and cycle numbers. The validity of the curve model is verified using ( $C_{\text{discharge}}$ ,  $\Delta V_{\text{charge}}$ ) data groups obtained from the charge-discharge cycle tests at different rates. The results indicate that the curve model can be effectively applied to predict the SOH of the Ni-MH batteries and the best prediction root-mean-square error (RMSE) can reach up to 1.2%. Further research is needed to confirm the application of this empirical curve model in practical fields.

**Keywords:** nickel-metal hydride (Ni-MH) battery; state-of-health (SOH); curve fitting; nonlinear least-squares method; prediction

## 1. Introduction

Nickel-metal hydride (Ni-MH) batteries have been applied in portable electronics and electric or hybrid-electric vehicles (EVs and HEVs) owing to their relatively good storage and power, higher safety, and excellent environmental acceptability [1–4]. With regard to these applications, the failure of Ni-MH batteries, resulting from irreversible capacity degradation and loss of performance in cycle service [5,6], is a key issue that warrants close attention. The state-of-health (SOH) status of a battery, which defines the current battery performance relative to its unused condition, is a powerful indicator of battery performance [7] and is usually used to predict the end-of-life and aging of batteries [8,9]. However, the definition of battery SOH is still somewhat equivocal [10] because different battery parameters can be used as the indicators of battery performance. This ambiguity makes the determination of battery SOH a difficult task.

Generally, three definitions of battery SOH have been reported, including SOH values based on battery impedance [11,12], battery capacity [9], and comprehensive battery parameters such as impedance, capacity, open circuit potential (OCV), charging or discharging current, and temperature ( $T$ ) [13–17]. Apparently, the SOH based on comprehensive battery parameters reflects the present battery performance more accurately, but it also makes the estimation more complicated. The SOH values based on battery impedance and capacity are considered to reflect the capability of

the battery to provide a certain power and to store energy, respectively. Both of the SOH values are widely applied in EVs and HEVs. In this case, all the methods for the estimation of battery impedance and battery capacity can be used as a basis for the SOH estimation. However, the estimations of battery impedance and battery capacity are also not easy to do, especially online estimation [18,19].

The reported methods for the estimation of battery SOH can be generally divided into two categories: physics-based model estimations and non-physics-based model estimations. Physics-based model estimations are based on electrical or electrochemical cell models [20–27]. In order to improve the estimation accuracy, some algorithms, such as adaptive observers [28], extended Kalman filter (EKF) [29,30], and relevance vector machines (RVMs)—particle filters (PFs) [31], are usually employed. The main problem for this kind of estimation is that the battery electrical or electrochemical models may not be unique and it is difficult to verify their validity. If the used cell model is not appropriate, the estimation accuracy may be lower and difficult to improve. In addition, the used algorithms are relatively complicated, which make it difficult to use them for online estimation.

In the non-physics-based model estimations, some learning algorithms, such as neural networks [32–34], support vector machines (SVMs) [35,36], RVMs [37], and fuzzy logic [38,39], are applied, in which the measured impedance parameters [12,32] and other characteristic battery parameters (e.g., discharge current [33], temperature, and state-of-charge (SOC) [34]) are employed as input variables. These methods can learn the battery behavior based on monitored data and thus do not demand battery physics models, but they need lots of training data and depend on the availability of a historic data set. In this case, it is difficult to use them for online estimations. Another kind of non-physics-based model estimation uses various curve equations between the practicable capacity and aging cycles [40–44], in which the parameters of the equations can be obtained by data fitting algorithms, and further they can be adjusted online by using a particle filtering (PF) approach [43] or by combining sets of training data based on Dempster-Shafer theory (DST) and the Bayesian Monte Carlo (BMC) method [44]. This method also needs a lot of accelerated aging test data to determine the curve equations, but it does not need complicated mathematic computations. In addition, the number of aging cycles of a used battery may be unknown in practical applications.

The purpose of this work is to find a simple model for the SOH prediction of Ni-MH batteries to avoid the problems mentioned above, such as the uncertainty of battery physics models, complicated algorithms, comprehensive parameters, and unknown cycle numbers. Therefore we tried to construct a simple curve model without electrical or electrochemical battery models and cycle numbers.

In this work, the SOH is defined as Equation (1) due to the presence of charge-discharge efficiency:

$$\text{SOH} = C_{\text{discharge}}/C_{\text{rated}} \quad (1)$$

where  $C_{\text{discharge}}$  (Ah) is the discharging capacity of fully charged Ni-MH batteries and  $C_{\text{rated}}$  (Ah) is the rated capacity. As the  $C_{\text{rated}}$  for one type of Ni-MH battery is a constant value, the SOH prediction is reduced to the prediction of  $C_{\text{discharge}}$ . Based on the analysis of a lot of charge-discharge cycle test data for commercial Ni-MH batteries, the voltage change in 1 s occurring at the start of the charging process ( $\Delta V_{\text{charge}}$ , mV) was selected as the characteristic parameter, and a curve equation between  $C_{\text{discharge}}$  and  $\Delta V_{\text{charge}}$  was determined to construct a curve model for the  $C_{\text{discharge}}$  prediction. Then the prediction precision of this curve model was verified by using some typical charge and discharge data for the Ni-MH batteries.

## 2. Experimental

Commercial AA-type Ni-MH cells (Pisen<sup>®</sup>, Sichuan, China,  $C_{\text{rated}} = 1.8$  Ah and rated voltage = 1.2 V) were used in this study. All charge-discharge tests were conducted using a computer-controlled charge-discharge instrument (BTS-3008-5V3A, Xinwei, Guangzhou, China) at room temperature ( $20 \pm 5$  °C). The charge-discharge data, including current ( $I$ ), potential ( $V$ ),

time ( $t$ ), and cycle number ( $n$ ), were recorded automatically with the sampling frequency of 1 Hz. The charge-discharge rates have significant influence on battery performance, so three different charge-discharge rates (0.5C, 1.0C, and 1.6C) were selected to simulate low, medium, and high charge-discharge rate conditions. The charge-discharge test program is described as follows:

The Ni-MH cells with initial SOC at 0% were fully charged at a constant current ( $I_{\text{charge}}$ : 0.5C, 1.0C, and 1.6C), then after an interval of 600 s, they were discharged at the same constant current ( $I_{\text{discharge}}$ : 0.5C, 1.0C, and 1.6C) to the cutoff voltage (0.9 V). After an interval of 1800 s, the next cycle of charge-discharge test was started. When the  $C_{\text{discharge}}$  of the test cells fell to 80% of the initial capacity, the charge-discharge tests were terminated [45]. The failure capacity is still defined as  $0.8C_{\text{rated}}$  in this paper for convenient applications.

### 3. Results and Discussion

#### 3.1. Curve Modeling for $C_{\text{discharge}}$

Figure 1 gives the typical  $I$ - $t$  and  $V$ - $t$  curves of two cycles for a Ni-MH battery in the charge-discharge test at 1.0C. In each cycle there are four abrupt voltage changes ( $\Delta V$ ) occurring at the start/end of the charging and discharging processes, respectively. According to the equivalent circuit of the test cell [8,46], these four  $\Delta V$  values in each cycle generally reflect the internal resistance ( $R_{\text{internal}}$ ) of the test cell in different states, and there is little difference among their values. However, the measurement of  $\Delta V$  is much easier than the test of  $R_{\text{internal}}$ , so it is selected as studied parameter. Before the start of the charging process, the completely discharged test cell was in a relatively stable state after the recovery of 1800 s, so in this paper we select the  $\Delta V$  in 1 s at the start of the charging process ( $\Delta V_{\text{charge}}$ , mV) as the characteristic parameter to verify its relationship with the aging state of the test cell, as shown in Figure 1.

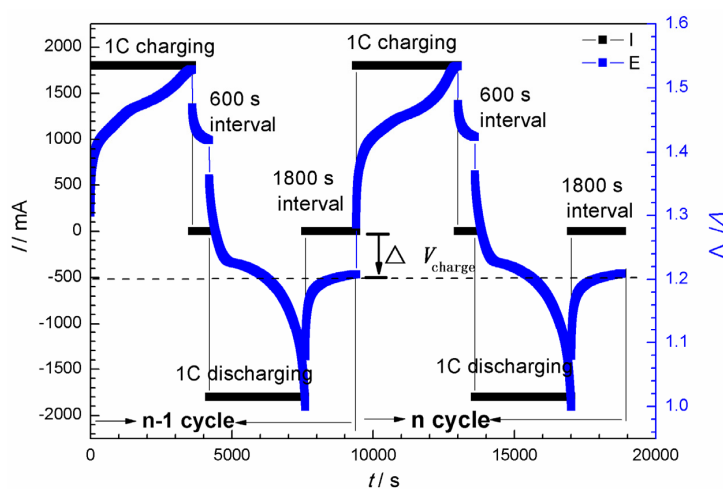


**Figure 1.** Typical  $I$ - $t$  and  $V$ - $t$  curves in the charge-discharge test at 1.0C for Ni-MH batteries (AA-type, 1.8 Ah, 1.2 V).

Through the analysis of the  $I$ - $t$  and  $V$ - $t$  data for each test battery, we obtained  $C_{\text{discharge}}$  and  $\Delta V_{\text{charge}}$  in each cycle. In order to observe the relationship of these three parameters, we made a three-dimensional (3D) diagram of  $(C_{\text{discharge}}-\Delta V_{\text{charge}}-n)$  for all the test Ni-MH batteries. Figure 2a shows a typical 3D diagram for a Ni-MH battery in the charge-discharge test at 1.0C and its two-dimensional (2D) projection diagrams  $(C_{\text{discharge}}-n, \Delta V_{\text{charge}}-n, C_{\text{discharge}}-\Delta V_{\text{charge}})$ .

From Figure 2a it can be seen that  $(C_{\text{discharge}}; \Delta V_{\text{charge}}; n)$  data points form a curve in the 3D space without obvious discrete point; suggesting that there would be nonlinear relationships between these three parameters. From the different 2D diagrams in Figure 2b–d; it can be seen more clearly that  $C_{\text{discharge}}-n$ ;  $\Delta V_{\text{charge}}-n$  and  $C_{\text{discharge}}-\Delta V_{\text{charge}}$  curves all display good nonlinear relationships. The

results in Figure 2b,c can be explained appropriately [41] and the nonlinear relationships between  $C_{\text{discharge}}^{-n}$  and  $\Delta V_{\text{charge}}^{-n}$  can be used to predict the state of Ni-MH batteries. However; sometimes the number of cycles for a Ni-MH battery is unknown. In this case; the nonlinear relationship between  $C_{\text{discharge}}$  and  $\Delta V_{\text{charge}}$ ; as shown in Figure 2d; is important for a curve model without cycle numbers. If we can obtain the relationship between  $C_{\text{discharge}}$  and  $\Delta V_{\text{charge}}$  for a Ni-MH battery; we can obtain its  $C_{\text{discharge}}$  through the measurement of its  $\Delta V_{\text{charge}}$  and then estimate its SOH with Equation (1).

Finally, we identified that Equation (2) can be used to describe the nonlinear relationship between  $\Delta V_{\text{charge}}$  (mV) and  $C_{\text{discharge}}$  (Ah):

$$C_{\text{discharge}} = \frac{a}{1 + \exp[-k \times (\Delta V_{\text{charge}} - c)]} \quad (2)$$

where  $a$  (Ah),  $k$  ( $\text{mV}^{-1}$ ) and  $c$  (mV) are constants related to test batteries. We found that  $k$  was negative with a small absolute value ( $|k|$ ) and related to the charge-discharge rate. In the initial cycles,  $\Delta V_{\text{charge}} \ll c$  and therefore, if  $|k|$  is not very small, there is,  $\exp[-k \times (\Delta V_{\text{charge}} - c)] \rightarrow 0$  and  $a \approx C_{\text{discharge}}$ . So  $a$  can be considered as a parameter related to the initial  $C_{\text{discharge}}$  of the test battery when  $|k|$  is not very small, which may be near its rated capacity. When  $\Delta V_{\text{charge}} = c$ ,  $C_{\text{discharge}} = 0.5a$ . Thus,  $c$  can be considered as a parameter related to the  $\Delta V_{\text{charge}}$  when  $C_{\text{discharge}}$  is at its 50% initial value.

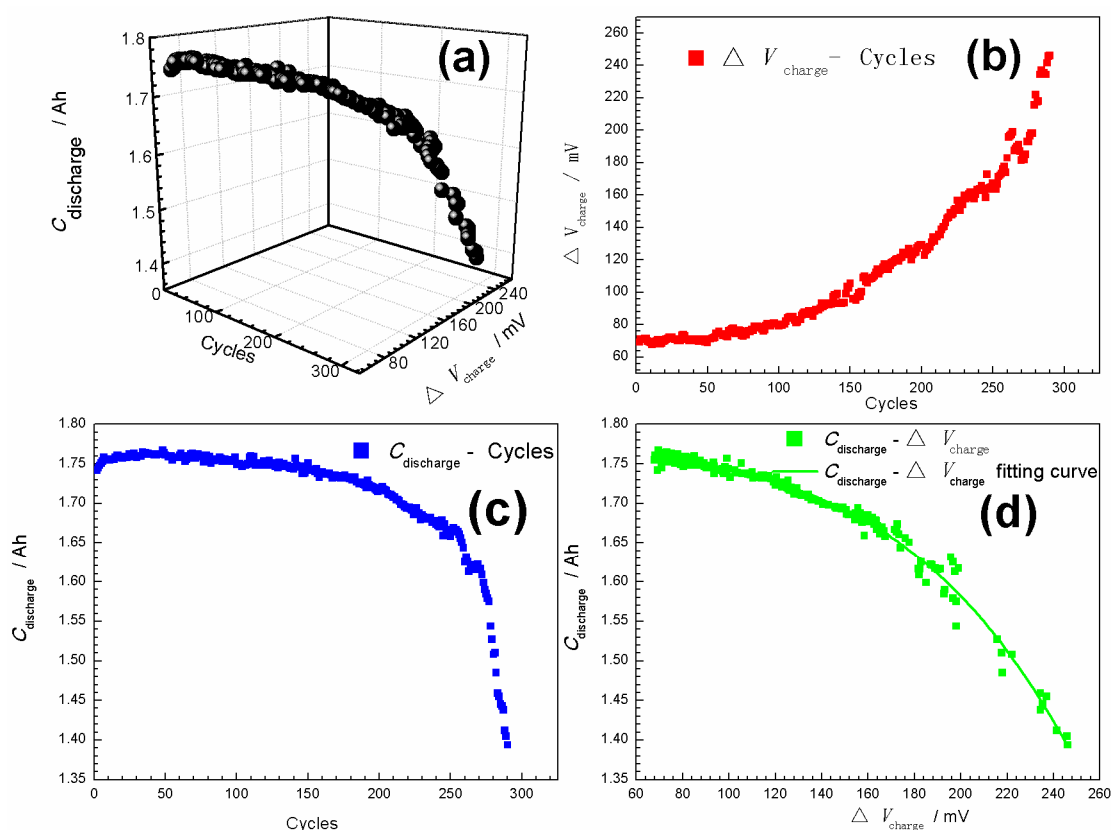


**Figure 2.** 3D diagram for a Ni-MH battery in the charge-discharge test at 1.0C (AA-type, 1.8 Ah, 1.2 V): (a) 3D diagram and (b), (c) and (d) projection of the 3D diagram.

The raw data in Figure 2d was fitted with Equation (2) by a nonlinear least-squares method, and the fitted curve indicates that it fits the raw data well. In order to verify the validity of Equation (2), different  $(C_{\text{discharge}}, \Delta V_{\text{charge}})$  raw data obtained from different Ni-MH batteries with different charge-discharge rates were fitted with Equation (2) by the nonlinear least-squares method.

Figure 3 shows some typical ( $C_{\text{discharge}}, \Delta V_{\text{charge}}$ ) raw data at different charge-discharge rates and their fitted curves with Equation (2). Table 1 lists the fitting parameters of  $a$ ,  $c$ , and  $k$  for different Ni-MH cells at different rates, in which  $R^2$  is a correlation coefficient and  $P_{\text{range}}$  is the selection range of initial values for each fitting parameter when using the nonlinear least-squares method to solve their values.

The results in Figure 3 and Table 1 prove that Equation (2) can well describe the relationship between  $C_{\text{discharge}}$  and  $\Delta V_{\text{charge}}$ . From Table 1, it can be seen that at 0.5C and 1.0C the parameter  $a$  is approximate to the rated capacity of the test Ni-MH batteries (1.8 Ah), while at 1.6C it becomes larger than the rated capacity because of the too small  $|k|$  value. It should be noted that at 1.6C the too small  $|k|$  value makes  $|-k \times (\Delta V_{\text{charge}} - c)| \ll 1$  and then, there is  $\exp[-k \times (\Delta V_{\text{charge}} - c)] \approx 1 - [k \times (\Delta V_{\text{charge}} - c)]$ . In this case, the nonlinear relationship between  $C_{\text{discharge}}$  and  $\Delta V_{\text{charge}}$  described with Equation (2) becomes an approximate linear relationship especially with an increase in  $\Delta V_{\text{charge}}$ , as shown in Figure 3.

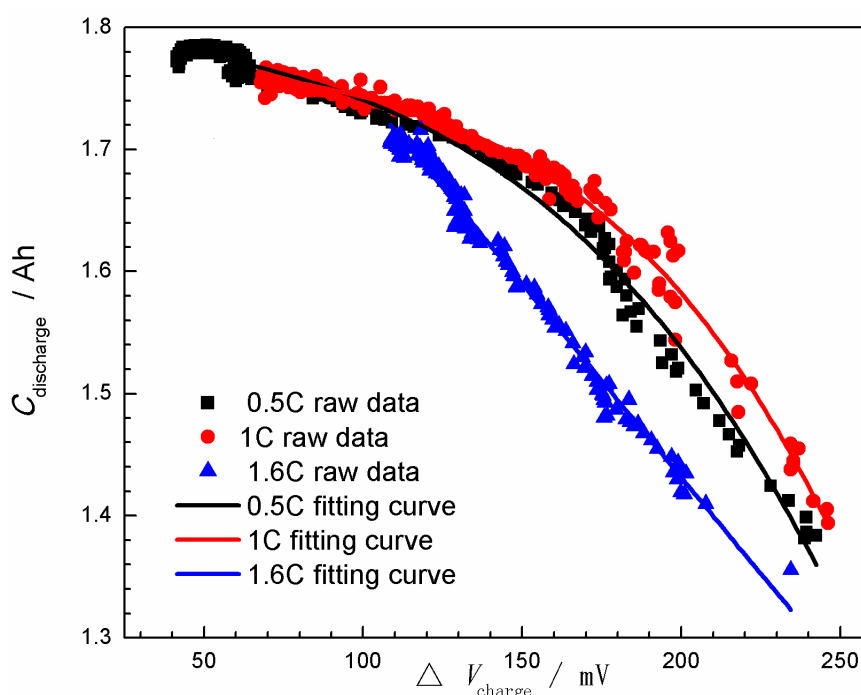


Figure 3. ( $C_{\text{discharge}}, \Delta V_{\text{charge}}$ ) raw data at different rates and their fitting curves with Equation (2).

Table 1. Fitting parameters of  $a$ ,  $c$ , and  $k$  for different Ni-MH cells at different rates.

| Rates | $a/\text{Ah}$      | $c/\text{mV}$ | $k/\text{mV}^{-1}$ | $R^2$    |        |
|-------|--------------------|---------------|--------------------|----------|--------|
| 0.5C  | $P_{\text{range}}$ | 1.5–2.0       | 200–400            | –0.02–0  | -      |
|       |                    | 1.8131        | 317.58             | –0.0146  | 0.9862 |
| 1.0C  | $P_{\text{range}}$ | 1.5–2.0       | 200–400            | –0.03–0  | -      |
|       |                    | 1.7828        | 320.26             | –0.0172  | 0.9882 |
|       |                    | 1.7420        | 310.20             | –0.0164  | 0.9851 |
|       |                    | 1.7680        | 223.30             | –0.0188  | 0.9796 |
|       |                    | 1.7839        | 286.11             | –0.0166  | 0.9800 |
|       |                    | 1.9433        | 313.77             | –0.0078  | 0.9865 |
| 1.6C  | $P_{\text{range}}$ | 2.0–3.0       | 200–400            | –0.015–0 | -      |
|       |                    | 2.4479        | 258.21             | –0.0057  | 0.9898 |
|       |                    | 2.6365        | 239.15             | –0.0048  | 0.9890 |

Apparently, the values of the  $a$ ,  $c$ , and  $k$  change with the charge-discharge rate. Table 1 shows that when the charge-discharge rate increases from 0.5C to 1.0C, the change of these three parameters is small, while at 1.6C the change of  $a$  and  $k$  is obvious. It may be speculated that the values of the three parameters just fluctuate slightly when the charge-discharge rate is in a certain range, such as 0.5C–1.0C. If so, this curve model should also be used in practical fields that the charge-discharge rates are not constant during applications. Further research will be conducted to verify the application of this curve model in practical fields. In this paper we just focus on the curve model itself and its SOH prediction accuracy.

### 3.2. State-of-Health (SOH) Prediction of Ni-MH Batteries Based on the Curve Model for $C_{\text{discharge}}$

When the relationship between  $C_{\text{discharge}}$  and  $\Delta V_{\text{charge}}$  of one battery is built as Equation (2), the  $C_{\text{discharge}}$  can be predicted by measuring the  $\Delta V_{\text{charge}}$  of the battery and then the SOH can be obtained with Equation (1). So we used the  $(C_{\text{discharge}}, \Delta V_{\text{charge}})$  raw data in Table 1 to check whether the curve model for  $C_{\text{discharge}}$  can be used for the SOH prediction.

Theoretically, only three groups of  $(C_{\text{discharge}}, \Delta V_{\text{charge}})$  data are needed to solve the three parameters in Equation (2). However, the measured raw data usually have some discrete points, as shown in Figures 2 and 3 so more groups of  $(C_{\text{discharge}}, \Delta V_{\text{charge}})$  data are needed and the prediction error is inevitable. In order to evaluate the prediction error, the root-mean-square error (RMSE) is defined as Equation (3):

$$RMSE = \sqrt{\sum_{j=1}^n [C_{\text{discharge},j} - C_{\text{discharge},j}^{\text{test}}]^2/n}, j = 1, \dots, n \quad (3)$$

where  $C_{\text{discharge},j}^{\text{test}}$  is the test value for sample  $j$ ;  $C_{\text{discharge},j}$  is the predicted value for sample  $j$ ; and  $n$  is the total number of samples.

The prediction method is described as follows:

(1) A certain number of  $(C_{\text{discharge}}, \Delta V_{\text{charge}})$  data groups in continuous charge-discharge test cycles were selected to fit the parameters in Equation (2) using a nonlinear least-squares method to obtain Equation (2) for the test Ni-MH battery;

(2) The predicted  $C_{\text{discharge}}$  values were calculated with Equation (2) using the tested  $\Delta V_{\text{charge}}$  values apart from those used in Step 1; and (3) the predicted RMSE was checked with Equation (3) using the predicted  $C_{\text{discharge}}$  values and the corresponding tested  $C_{\text{discharge}}$  values. Through the predicted RMSE we can judge how large the prediction error is and whether the prediction is valid.

Using different numbers of  $(C_{\text{discharge}}, \Delta V_{\text{charge}})$  data groups in different parts of the  $C_{\text{discharge}}-\Delta V_{\text{charge}}$  curve, as shown in Figure 4, may result in different prediction results. In this paper, the first cycle  $C_{\text{discharge}}$  of a selected  $(C_{\text{discharge}}, \Delta V_{\text{charge}})$  data group ( $C_{\text{discharge}}^0$ ) is described with the SOH value of the test battery, and a relative capacity drop (RCd) is defined to describe the variation range of  $C_{\text{discharge}}$  in the selected  $(C_{\text{discharge}}, \Delta V_{\text{charge}})$  data group, as presented in Equation (4):

$$RCd = \frac{C_{\text{discharge}}^0 - C_{\text{discharge}}^n}{C_{\text{discharge}}^0} \quad (4)$$

where  $C_{\text{discharge}}^n$  is the last cycle  $C_{\text{discharge}}$  of the selected  $(C_{\text{discharge}}, \Delta V_{\text{charge}})$  data group. Apparently, the RCd value determines the last  $(C_{\text{discharge}}, \Delta V_{\text{charge}})$  data of the selected data group. Because we used all the  $(C_{\text{discharge}}, \Delta V_{\text{charge}})$  data in continuous test cycles, a larger RCd value means more data in the selected data group. In this case, the SOH and RCd values for a selected data group can determine its position on the  $C_{\text{discharge}}-\Delta V_{\text{charge}}$  curve and also indicate the corresponding battery states.

Firstly, the effect of the number of used  $(C_{\text{discharge}}, \Delta V_{\text{charge}})$  data groups, which is described by RCd, on the prediction of  $C_{\text{discharge}}$  is investigated. Figure 4 shows a 3D diagram of  $(C_{\text{discharge}}-\Delta V_{\text{charge}}-n)$  for a Ni-MH battery in the charge-discharge test at 1.0C and the predicted results obtained with SOH = 97.38% and different RCds (0.5%, 1.0%, and 1.5%), in which the

corresponding cycle numbers of the selected data range and the prediction *RMSE* values are also listed. In Figure 4, the three data groups are selected from 90–138 cycles (48 data), 90–166 cycles (77 data), and 90–184 cycles (95 data), respectively. The first cycle of the three date groups is the same, so they have the same SOH value (97.38%). Their RCd values are calculated with Equation (4) using the  $C_{\text{discharge}}$  of the 90th cycle (*i.e.*,  $C_{\text{discharge}}^0$ ) and  $C_{\text{discharge}}^{138}$ ,  $C_{\text{discharge}}^{166}$ , and  $C_{\text{discharge}}^{184}$ , respectively. It is seen that the prediction *RMSE* value decreases with an increase in RCd, suggesting that using more ( $C_{\text{discharge}}, \Delta V_{\text{charge}}$ ) data groups may decrease the prediction error.

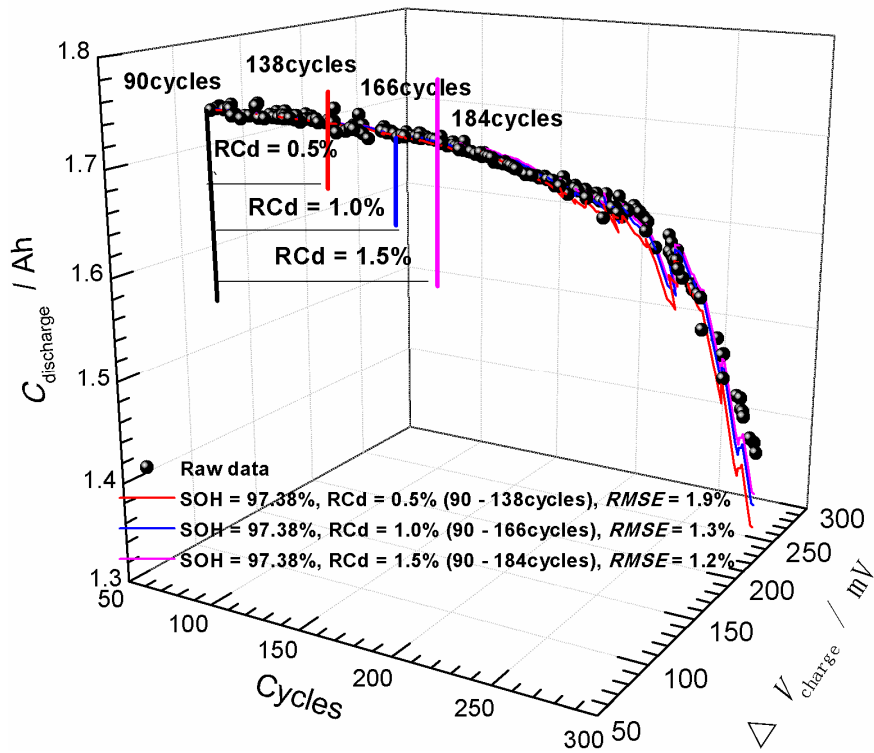


**Figure 4.** 3D diagram of ( $C_{\text{discharge}} - \Delta V_{\text{charge}} - n$ ) for a Ni-MH battery in the charge-discharge test at 1.0C and the prediction curves obtained with SOH = 97.38% and different relative capacity drops (RCds) (0.5%, 1.0%, and 1.5%).

The SOH value of the selected data group, *i.e.*, the position of the starting point of the selected data group, may also influence the prediction result. So we selected data groups at different SOH with various RCds (0.5%, 1.0%, 1.5%, and 2.0%) to fit the parameters in Equation (2) and calculated the corresponding prediction *RMSE* values, as shown in Figure 5.

In Figure 5, the average *RMSE* value at each SOH is presented and shown with a star symbol, while the general average *RMSE* value ( $\overline{RMSE}$ ) is also given and shown with a horizontal dashed line. The *RMSE* value obtained by using data groups at SOH = 94.89% with RCd = 0.5% deviates significantly from other *RMSE* values, which may be due to the fluctuation of the raw data groups, so it was eliminated from the calculation of the average *RMSE* values.

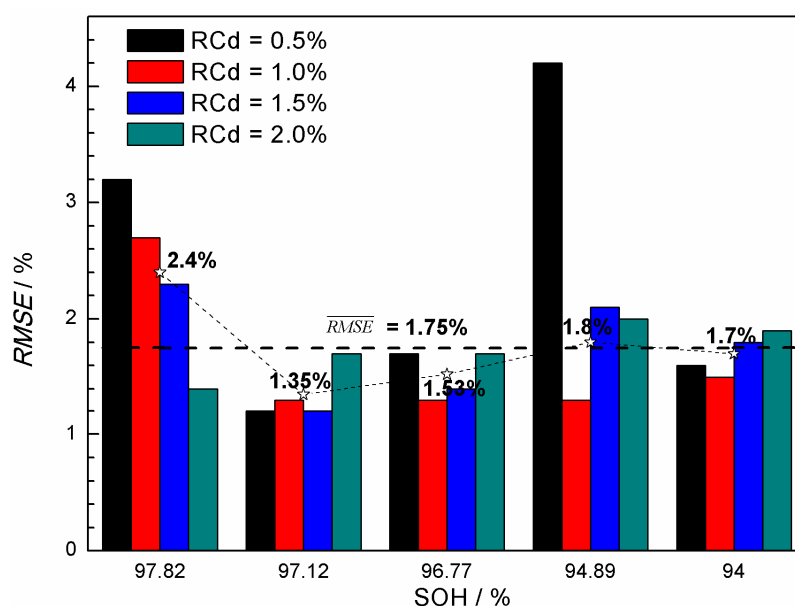


**Figure 5.** Prediction root-mean-square error ( $RMSE$ ) for a Ni-MH battery in the charge-discharge test at 1.0C using ( $C_{\text{discharge}}$ ,  $\Delta V_{\text{charge}}$ ) data groups at different SOH with various RCds.

From Figure 5, it can be seen that when  $SOH = 97.82\%$ , the prediction  $RMSE$  decreases obviously with an increase in RCd, which is consistent with the result in Figure 4. But when the SOH value decreases to 97.12%, 96.77%, 94.89%, and 94%, at each SOH the prediction  $RMSE$  does not decrease with an increase in RCd, suggesting that using more data groups does not necessarily help improve the prediction precision. In addition, the prediction  $RMSE$  does not show some regular change with a decrease in the SOH, but generally it seems that when the SOH is in an intermediate range (97.12% and 96.77%), the prediction  $RMSE$  is relatively lower.

Figure 6 shows the selected ( $C_{\text{discharge}}$ ,  $\Delta V_{\text{charge}}$ ) raw data in Figure 5 and the prediction data with the best  $RMSE$  (1.2%) and the  $RMSE$  (1.7%) near the  $\overline{RMSE}$  in Figure 5 (1.75%).

From Figure 6, we can clearly see that the prediction data well accords with the raw data, especially when  $C_{\text{discharge}} > 1.44$  Ah, *i.e.*, before the failure capacity ( $0.8C_{\text{rated}}$ ), indicating that the prediction accuracy of this curve model is satisfied. It should be noted that the initial part of the raw data in Figure 6 ( $SOH > 97.12\%$ ) has some volatility. So using this part of the raw data for the  $C_{\text{discharge}}$  prediction may result in higher prediction error (*i.e.*, large  $RMSE$ ) and using more data groups (*i.e.*, large RCd) may improve the prediction precision, as shown in Figure 5 at  $SOH = 97.82\%$ . When the SOH decreases to 97.12%–96.77%, the fluctuation of the raw data decreases, as shown in Figure 6; this may result in lower prediction  $RMSE$ , as shown in Figure 5.

Considering the influence of different charge-discharge rates on the prediction results, we selected the ( $C_{\text{discharge}}$ ,  $\Delta V_{\text{charge}}$ ) raw data at 0.5C and 1.6C to check the curve model using the same method described above. Figure 7 shows the prediction  $RMSE$  for a Ni-MH battery in the charge-discharge test at 0.5C using ( $C_{\text{discharge}}$ ,  $\Delta V_{\text{charge}}$ ) data groups at different SOH with various RCds, in which the average prediction  $RMSE$  values are also given as described in Figure 5. The  $RMSE$  values at  $SOH = 98.97\%$  are relative large, which may also result from the fluctuation in the initial data groups, so they are eliminated from the calculation of the  $\overline{RMSE}$  in Figure 7.

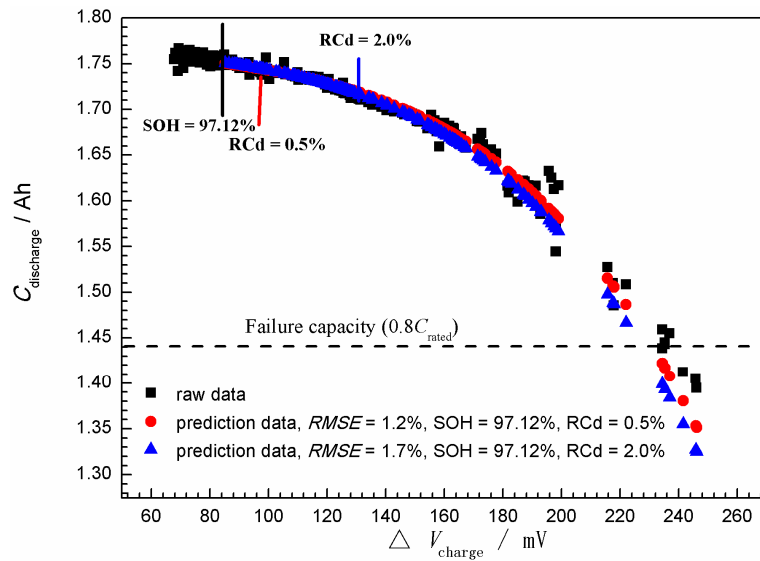


**Figure 6.** ( $C_{\text{discharge}}, \Delta V_{\text{charge}}$ ) raw data used in Figure 5 and the prediction data with the best  $RMSE$  (1.2%) and the  $RMSE$  (1.7%) near the  $\overline{RMSE}$  in Figure 5 (1.75%).

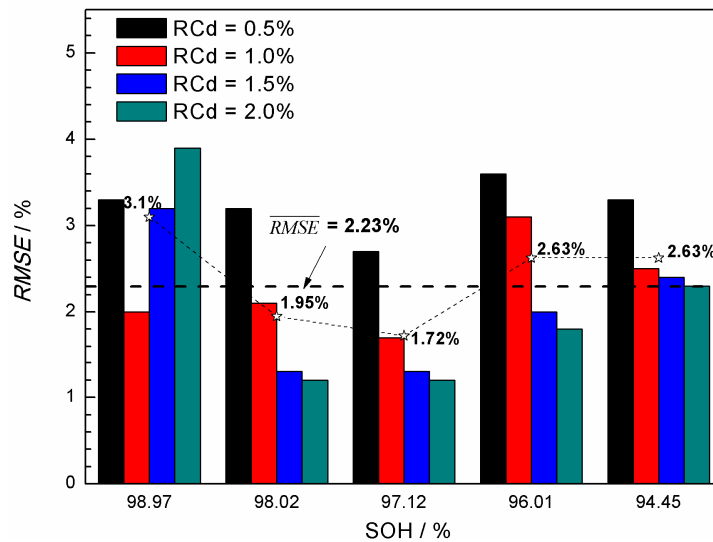


**Figure 7.** Prediction  $RMSE$  for a Ni-MH battery in the charge-discharge test at 0.5C using ( $C_{\text{discharge}}, \Delta V_{\text{charge}}$ ) data groups at different state-of-health (SOH) with different RCds.

From Figure 7, it can be seen that at SOH = 98.97% the prediction  $RMSE$  is higher and does not decrease with an increase in RCd, while at lower SOH values (98.02%–94.45%) the prediction  $RMSE$  decreases with an increase in RCd. In general, it seems that when the SOH is in an intermediate range (98.02% and 97.12%), the prediction  $RMSE$  is relatively lower, which is consistent with the results in Figure 5.

Figure 8 presents the ( $C_{\text{discharge}}, \Delta V_{\text{charge}}$ ) raw data used in Figure 7 and the prediction data with the best  $RMSE$  (1.2%) and the  $RMSE$  (2.1%) near the  $\overline{RMSE}$  in Figure 7 (2.23%). Similarly, there is fluctuation in the initial part of the ( $C_{\text{discharge}}, \Delta V_{\text{charge}}$ ) raw data and the prediction data well accords with the raw data before the failure capacity.

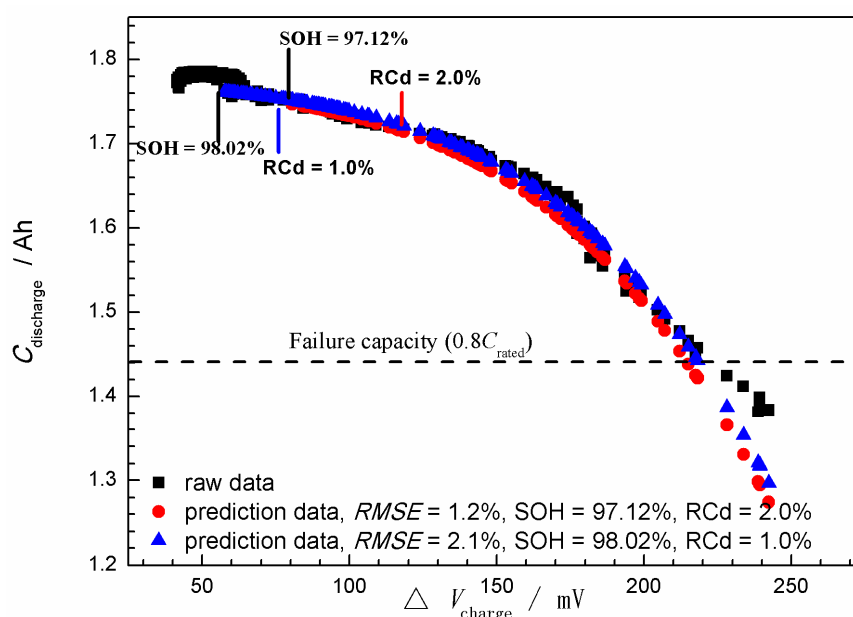
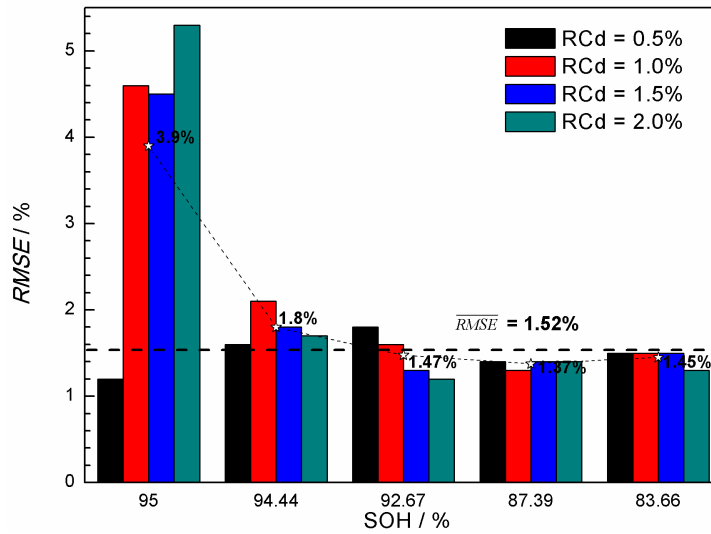


**Figure 8.** ( $C_{\text{discharge}}, \Delta V_{\text{charge}}$ ) raw data used in Figure 7 and the prediction data with the best  $RMSE$  (1.2%) and the  $RMSE$  (2.1%) near the  $\overline{RMSE}$  in Figure 7 (2.23%).

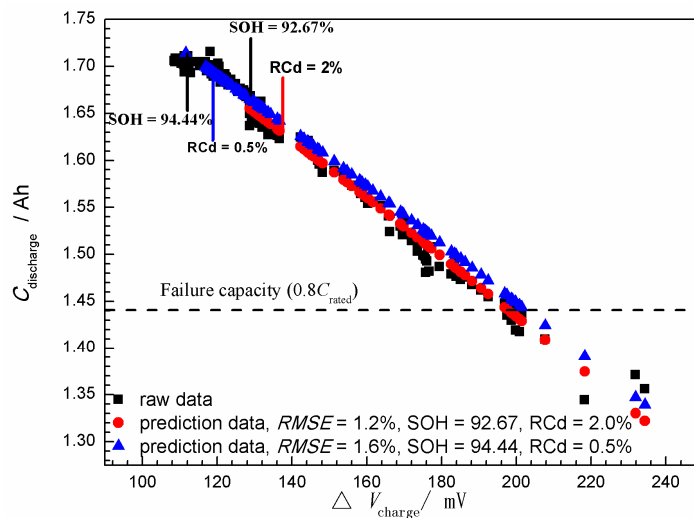
Figure 9 shows the prediction  $RMSE$  for a Ni-MH battery in the charge-discharge test at 1.6C, in which the average prediction  $RMSE$  values are also given as described in Figure 5. Similarly, the  $RMSE$  values at  $SOH = 95\%$  are eliminated from the calculation of the  $\overline{RMSE}$  value in Figure 9.

Figure 10 presents the ( $C_{\text{discharge}}, \Delta V_{\text{charge}}$ ) raw data used in Figure 9 and the prediction data with the best  $RMSE$  (1.2%) and the  $RMSE$  (1.6%) near the  $\overline{RMSE}$  in Figure 9 (1.53%). It can be seen that there is an obvious increase in the  $C_{\text{discharge}}$  value in the initial charge-discharge period, as shown in Figure 10, so these data groups cannot be used for the prediction. As shown in Figure 9, only when the  $SOH < 95\%$ , the prediction  $RMSE$  decreases to a lower value and the prediction data also accords well with the raw data before the failure capacity, as shown in Figure 10.

The results in Figures 4–10 indicate that the curve model based on Equation (2) can be effectively applied to predict the  $SOH$  of the Ni-MH batteries, and the best prediction  $RMSE$  is around 1.2%. The selected raw data groups for the prediction significantly influence the prediction  $RMSE$ . Generally, the data groups in the early period of the charge-discharge test, which depends on the charge-discharge rate, are not suitable for the  $SOH$  prediction because of data fluctuations. Increasing the  $RCd$  value, *i.e.*, using more data groups for the  $SOH$  prediction, does not necessarily help improve the prediction precision, which may also be related to the data fluctuation. Generally, using data groups at the  $SOH$  in an intermediate range and with the  $RCd$  value in the range of 1.5%–2.0% may result in lower prediction  $RMSE$ .



**Figure 9.** Prediction  $RMSE$  for a Ni-MH battery in the charge-discharge test at 1.6C using  $(C_{\text{discharge}}, \Delta V_{\text{charge}})$  data groups at different SOH with various RCds.



**Figure 10.**  $(C_{\text{discharge}}, \Delta V_{\text{charge}})$  raw data used in Figure 9 and the prediction data with the best  $RMSE$  (1.2%) and the  $RMSE$  (1.6%) near the  $RMSE$  in Figure 9 (1.52%).

Apart from good prediction accuracy, this curve model is also simple and easy-to-use. These advantages are important for online applications. For any type of Ni-MH battery, we can use charge-discharge cycle tests to determine the three parameters ( $a$ ,  $c$ , and  $k$ ) in the curve model at different charge-discharge rates. Then, we can easily detect the SOH of the same type Ni-MH batteries without considering their aging history (e.g., cycle numbers). As shown in Table 1, the three parameters for different batteries change a little in a certain range of charge-discharge rates, such as 0.5–1.0C. In this case, it is possible to use their average values to construct a general model for the applications with fluctuated charge-discharge rates. Moreover, if more than three  $(C_{\text{discharge}}, \Delta V_{\text{charge}})$  data can be obtained during applications, the new values of the three parameters ( $a$ ,  $c$ , and  $k$ ) can be calculated to modify the general curve model. Certainly, this application of the curve model is needed further verification.

One of limitations for this curve model is that it's relatively higher prediction error in a higher SOH range especially at higher charge-discharge rates. In addition, it should be noted that in this

work the ( $C_{\text{discharge}}$ ,  $\Delta V_{\text{charge}}$ ) data obtained from the charge-discharge cycle test were employed to construct the curve model and to verify its validity for the SOH prediction. In practical applications, batteries may undertake nonuniform charge-discharge processes, such as intermittent charge or discharge processes. Therefore, further research is needed to confirm whether this curve model can continue to be used for any Ni-MH battery in practical applications.

#### 4. Conclusions

Based on charge-discharge cycle tests for commercial Ni-MH batteries (Pisen<sup>®</sup>, 1.2 V, 1.8 Ah), a curve model was constructed without battery models and cycle numbers for the SOH prediction and its prediction precision was verified. The main conclusions were drawn as follows:

- (1) Based on the analysis of charge-discharge data for the Ni-MH batteries, a nonlinear relationship between the  $C_{\text{discharge}}$  (Ah) and  $\Delta V_{\text{charge}}$  (mV) was found and described as  $C_{\text{discharge}} = a/[1 + \exp[-k \times (\Delta V_{\text{charge}} - c)]]$ , where  $a$  (Ah),  $k$  ( $\text{mV}^{-1}$ ) and  $c$  (mV) are constants related to charge-discharge rates. Based on this equation, the curve model for the SOH prediction of Ni-MH batteries was constructed.
- (2) The ( $C_{\text{discharge}}$ ,  $\Delta V_{\text{charge}}$ ) data groups obtained from the charge-discharge cycle test at different rates (0.5C, 1.0C, and 1.6C) were employed to verify the validity of the curve model for the SOH prediction. It was found that the curve model based on the nonlinear relationship between the  $C_{\text{discharge}}$  and  $\Delta V_{\text{charge}}$  can be effectively applied to predict the SOH of the Ni-MH batteries. The data groups used for the SOH prediction have significantly influence on the prediction accuracy, and the best prediction RMSE can reach 1.2%.
- (3) Generally, using ( $C_{\text{discharge}}$ ,  $\Delta V_{\text{charge}}$ ) data groups with the SOH in an intermediate range and with the RCd value in the range of 1.5%–2.0% may result in lower prediction RMSE.

**Acknowledgments:** The authors thank the Special Funds for Basic Research of National Universities (No. 2015TS147) for the financial support of this work.

**Conflicts of Interest:** The authors declare no conflict of interest.

#### References

1. Leblanc, P.; Blanchard, P.; Senyarich, S. Self-Discharge of Sealed Nickel-Metal Hydride Batteries Mechanisms and Improvements. *J. Electrochem. Soc.* **1998**, *145*, 844–847. [[CrossRef](#)]
2. Yao, M.; Okuno, K.; Iwaki, T.; Tanase, S.; Harada, K.; Kato, M.; Emura, K.; Sakai, T. High-power nickel/metal-hydride battery using new micronetwork substrate: Discharge rate capability and cycle-life performance. *J. Power Sources* **2007**, *171*, 1033–1039. [[CrossRef](#)]
3. Fetcenko, M.; Ovshinsky, S.; Reichman, B.; Young, K.; Fierro, C.; Koch, J.; Zallen, A.; Mays, W.; Ouchi, T. Recent advances in Ni-MH battery technology. *J. Power Sources* **2007**, *165*, 544–551. [[CrossRef](#)]
4. Castro, E.; Cuscueta, D.; Milocco, R.; Ghilarducci, A.; Salva, H. An EIS based study of a Ni-MH battery prototype. Modeling and identification analysis. *Int. J. Hydrog. Energy* **2010**, *35*, 5991–5998. [[CrossRef](#)]
5. Serrao, L.; Chehab, Z.; Guezennec, Y.; Rizzoni, G. An aging model of Ni-MH batteries for hybrid electric vehicles. In Proceedings of the 2005 IEEE Conference Vehicle Power and Propulsion, Chicago, IL, USA, 7–9 September 2005; pp. 78–85.
6. Chehab, Z.; Serrao, L.; Guezennec, Y.G.; Rizzoni, G. Aging Characterization of Nickel: Metal Hydride Batteries Using Electrochemical Impedance Spectroscopy. In Proceedings of the International Mechanical Engineering Congress and Exposition, Chicago, IL, USA, 5–10 November 2006; pp. 343–349.
7. Salkind, A.J.; Fennie, C.; Singh, P.; Atwater, T.; Reisner, D.E. Determination of state-of-charge and state-of-health of batteries by fuzzy logic methodology. *J. Power Sources* **1999**, *80*, 293–300. [[CrossRef](#)]
8. Chiang, Y.H.; Sean, W.Y.; Ke, J.C. Online estimation of internal resistance and open-circuit voltage of lithium-ion batteries in electric vehicles. *J. Power Sources* **2011**, *196*, 3921–3932. [[CrossRef](#)]
9. Ng, K.S.; Moo, C.S.; Chen, Y.P.; Hsieh, Y.C. Enhanced coulomb counting method for estimating state-of-charge and state-of-health of lithium-ion batteries. *Appl. Energy* **2009**, *86*, 1506–1511. [[CrossRef](#)]

10. Waag, W.; Fleischer, C.; Sauer, D.U. Critical review of the methods for monitoring of lithium-ion batteries in electric and hybrid vehicles. *J. Power Sources* **2014**, *258*, 321–339. [[CrossRef](#)]
11. Huet, F. A review of impedance measurements for determination of the state-of-charge or state-of-health of secondary batteries. *J. Power Sources* **1998**, *70*, 59–69. [[CrossRef](#)]
12. Blanke, H.; Bohlen, O.; Buller, S.; de Doncker, R.W.; Fricke, B.; Hammouche, A.; Linzen, D.; Thele, M.; Sauer, D.U. Impedance measurements on lead-acid batteries for state-of-charge, state-of-health and cranking capability prognosis in electric and hybrid electric vehicles. *J. Power Sources* **2005**, *144*, 418–425. [[CrossRef](#)]
13. Liu, G.; Ouyang, M.; Lu, L.; Li, J.; Han, X. Online estimation of lithium-ion battery remaining discharge capacity through differential voltage analysis. *J. Power Sources* **2015**, *274*, 971–989. [[CrossRef](#)]
14. Sauer, D.U.; Wenzl, H. Comparison of different approaches for lifetime prediction of electrochemical systems—Using lead-acid batteries as example. *J. Power Sources* **2008**, *176*, 534–546. [[CrossRef](#)]
15. Zhu, J.; Sun, Z.; Wei, X.; Dai, H. A new lithium-ion battery internal temperature on-line estimate method based on electrochemical impedance spectroscopy measurement. *J. Power Sources* **2015**, *274*, 990–1004. [[CrossRef](#)]
16. Wenzl, H.; Baring-Gould, I.; Kaiser, R.; Liaw, B.Y.; Lundsager, P.; Manwell, J.; Ruddell, A.; Svoboda, V. Life prediction of batteries for selecting the technically most suitable and cost effective battery. *J. Power Sources* **2005**, *144*, 373–384. [[CrossRef](#)]
17. Ramadass, P.; Haran, B.; White, R.; Popov, B.N. Capacity fade of Sony 18650 cells cycled at elevated temperatures: Part II. Capacity fade analysis. *J. Power Sources* **2002**, *112*, 614–620. [[CrossRef](#)]
18. Bundy, K.; Karlsson, M.; Lindbergh, G.; Lundqvist, A. An electrochemical impedance spectroscopy method for prediction of the state of charge of a nickel-metal hydride battery at open circuit and during discharge. *J. Power Sources* **1998**, *72*, 118–125. [[CrossRef](#)]
19. Meissner, E.; Richter, G. Battery monitoring and electrical energy management: Precondition for future vehicle electric power systems. *J. Power Sources* **2003**, *116*, 79–98. [[CrossRef](#)]
20. Santhanagopalan, S.; Guo, Q.; Ramadass, P.; White, R.E. Review of models for predicting the cycling performance of lithium ion batteries. *J. Power Sources* **2006**, *156*, 620–628. [[CrossRef](#)]
21. Gao, L.; Liu, S.; Dougal, R.A. Dynamic lithium-ion battery model for system simulation. *IEEE Trans. Compon. Packag. Technol.* **2002**, *25*, 495–505.
22. Rao, R.; Vrudhula, S.; Rakhmatov, D.N. Battery modeling for energy aware system design. *Computer* **2003**, *36*, 77–87.
23. González-Longatt, F.M. Circuit based battery models: A review. In Proceedings of the 2nd Congreso Iberoamericano De Estudiantes de Ingeniería Eléctrica, Puerto la Cruz, Venezuela, 3–7 April 2006; pp. 1–5.
24. Chen, M.; Rincon-Mora, G.A. Accurate electrical battery model capable of predicting runtime and IV performance. *IEEE Trans. Energy Convers.* **2006**, *21*, 504–511. [[CrossRef](#)]
25. Zhu, W.H.; Zhu, Y.; Tatarchuk, B.J. A simplified equivalent circuit model for simulation of Pb-acid batteries at load for energy storage application. *Energy Convers. Manag.* **2011**, *52*, 2794–2799. [[CrossRef](#)]
26. Pascoe, P.E.; Anbuky, A.H. A unified discharge voltage characteristic for VRLA battery capacity and reserve time estimation. *Energy Convers. Manag.* **2004**, *45*, 277–302. [[CrossRef](#)]
27. Pascoe, P.E.; Anbuky, A.H. A VRLA battery simulation model. *Energy Convers. Manag.* **2004**, *45*, 1015–1041. [[CrossRef](#)]
28. Chiang, Y.H.; Sean, W.Y. Dynamical estimation of state-of-health of batteries by using adaptive observer. In Proceedings of the 2nd International Conference on Power Electronics and Intelligent Transportation System, 19–20 December 2009; pp. 110–115.
29. Hu, C.; Youn, B.D.; Chung, J. A multiscale framework with extended Kalman filter for lithium-ion battery SOC and capacity estimation. *Appl. Energy* **2012**, *92*, 694–704. [[CrossRef](#)]
30. Sepasi, S.; Ghorbani, R.; Liaw, B.Y. A novel on-board state-of-charge estimation method for aged Li-ion batteries based on model adaptive extended Kalman filter. *J. Power Sources* **2014**, *245*, 337–344. [[CrossRef](#)]
31. Saha, B.; Goebel, K.; Poll, S.; Christophersen, J. Prognostics methods for battery health monitoring using a Bayesian framework. *IEEE Trans. Instrum. Meas.* **2009**, *58*, 291–296. [[CrossRef](#)]
32. Chang, W.Y. Estimation of the state of charge for a LFP battery using a hybrid method that combines a RBF neural network, an OLS algorithm and AGA. *Int. J. Electr. Power Energy Syst.* **2013**, *53*, 603–611. [[CrossRef](#)]

33. Gorman, C.; Ingersoll, D.; Jungst, R.; Paez, T.L. Artificial neural network simulation of battery performance. In Proceedings of the Thirty-First Hawaii International Conference, Kohala Coast, HI, USA, 6–9 January 1998; pp. 115–121.
34. Andre, D.; Nuhic, A.; Soczka-Guth, T.; Sauer, D. Comparative study of a structured neural network and an extended Kalman filter for state of health determination of lithium-ion batteries in hybrid electric vehicles. *Eng. Appl. Artif. Intell.* **2013**, *26*, 951–961. [[CrossRef](#)]
35. Rufus, F.; Lee, S.; Thakker, A. Health monitoring algorithms for space application batteries. In Proceedings of the Prognostics and Health Management, Denver, CO, USA, 6–9 October 2008; pp. 1–8.
36. Widodo, A.; Shim, M.C.; Caesarendra, W.; Yang, B.S. Intelligent prognostics for battery health monitoring based on sample entropy. *Expert Syst. Appl.* **2011**, *38*, 11763–11769. [[CrossRef](#)]
37. Xing, Y.; Ma, E.W.; Tsui, K.L.; Pecht, M. Battery management systems in electric and hybrid vehicles. *Energies* **2011**, *4*, 1840–1857. [[CrossRef](#)]
38. Singh, P.; Fennie, C.; Reisner, D. Fuzzy logic modelling of state-of-charge and available capacity of nickel/metal hydride batteries. *J. Power Sources* **2004**, *136*, 322–333. [[CrossRef](#)]
39. Singh, P.; Kaneria, S.; Broadhead, J.; Wang, X.; Burdick, J. Fuzzy logic estimation of SOH of 125Ah VRLA batteries. In Proceedings of the International Telecommunications Energy Conference, Chicago, IL, USA, 19–23 September 2004; pp. 524–531.
40. Micea, M.V.; Ungurean, L.; Carstoiu, G.N.; Groza, V. Online state-of-health assessment for battery management systems. *IEEE Instrum. Meas.* **2011**, *60*, 1997–2006. [[CrossRef](#)]
41. Wang, F.; Fan, B.; Liu, S.; Qian, G.; Huang, X.; Han, S. Attenuation test and duplication of power battery's cycle life. *J. Automot. Saf. Energy* **2012**, *3*, 71–76.
42. Kang, L.; Zhao, X.; Ma, J. A new neural network model for the state-of-charge estimation in the battery degradation process. *Appl. Energy* **2014**, *121*, 20–27. [[CrossRef](#)]
43. Xing, Y.; Ma, E.W.; Tsui, K.-L.; Pecht, M. An ensemble model for predicting the remaining useful performance of lithium-ion batteries. *Microelectron. Reliab.* **2013**, *53*, 811–820. [[CrossRef](#)]
44. He, W.; Williard, N.; Osterman, M.; Pecht, M. Prognostics of lithium-ion batteries based on Dempster-Shafer theory and the Bayesian Monte Carlo method. *J. Power Sources* **2011**, *196*, 10314–10321. [[CrossRef](#)]
45. Eom, S.W.; Kim, M.K.; Kim, I.J.; Moon, S.I.; Sun, Y.K.; Kim, H.S. Life prediction and reliability assessment of lithium secondary batteries. *J. Power Sources* **2007**, *174*, 954–958. [[CrossRef](#)]
46. Remmlinger, J.; Buchholz, M.; Meiler, M.; Bernreuter, P.; Dietmayer, K. State-of-health monitoring of lithium-ion batteries in electric vehicles by on-board internal resistance estimation. *J. Power Sources* **2011**, *196*, 5357–5363. [[CrossRef](#)]



© 2015 by the authors; licensee MDPI, Basel, Switzerland. This article is an open access article distributed under the terms and conditions of the Creative Commons by Attribution (CC-BY) license (<http://creativecommons.org/licenses/by/4.0/>).